CrystEngComm

Nine isomorphous lanthanide-uranyl f-f bimetallic materials with 2-thiophenecarboxylic acid and terpyridine: structure and concomitant luminescent properties

Journal:	*CrystEngComm*
Manuscript ID	CE-ART-05-2018-000811.R1
Article Type:	Paper
Date Submitted by the Author:	18-Jul-2018
Complete List of Authors:	Ridenour, James; The George Washington University, Chemistry; Cahill, Chris; The George Washington University, Chemistry

Nine isomorphous lanthanide-uranyl f-f bimetallic materials with 2-thiophenecarboxylic acid and terpyridine: structure and concomitant luminescent properties

J. August Ridenour and Christopher L. Cahill*

Department of Chemistry, The George Washington University, 800 22nd Street, NW, Washington, D.C. 20052, United States

Abstract

A series of nine new 4f-5f lanthanide-uranyl complexes, $\{[(UO_2)_2(O)(L^1)(L^2)_2][UO_2(L^1)_3][Ln(L^1)_3(L^2)] \cdot H_2O\}_2$, (where L^1 and L^2 are 2-thiophenecarboxylic acid ($C_5H_3SO_2$) and 2,2':6'2"-terpyridine ($C_{15}H_{11}N_3$), respectively, and Ln = Pr^{3+} (**1**), Nd^{3+} (**2**), Sm^{3+} (**3**), Eu^{3+} (**4**), Gd^{3+} (**5**), Tb^{3+} (**6**), Dy^{3+} (**7**), Ho^{3+} (**8**), Er^{3+} (**9**)), and a uranyl only complex (**10**), $[(UO_2)_2(O)(L^1)(L^2)_2]_2[UO_2(L^1)_3] \cdot NO_3 \cdot H_2O$, have been hydrothermally synthesized and characterized with single crystal and powder X-ray diffraction. The nine bimetallic complexes are isomorphous, where only the identity of the lanthanide metal center changes, and contain two distinct uranyl units: a monomer with a formal negative charge and a dimer with a formal positive charge, as well as a single neutral dimeric lanthanide unit. The uranyl only phase (**10**) contains two unique dimers and a monomer, both similar to the units observed in the heterometallic series. Comparative analyses of speciation and the first coordination spheres between of title complexes and building units in the literature reveal common motifs and a possible structural influence of uranyl units. Further, the units in all complexes are held together primarily through weak hydrogen and offset π-stacking interactions. Raman and visible luminescent spectroscopic techniques found concurrent and selective emission from the uranyl and lanthanide metal centers in certain compounds.

Introduction

Research in heterometallic materials chemistry has been and remains an incredibly diverse and fruitful route for obtaining novel structural topologies and interesting, advantageous properties for materials in the realms of organometallics,[1, 2] clusters,[3, 4] and metal-organic hybrid compounds.[5, 6] These properties include a broad range of phenomena from photoelectric effects[7] and photocatalytic behavior[8] to luminescent properties[9] in emissive probes[10] and magnetism in single molecule magnets.[11] They arise from an additive or complementary amalgamation of the inherent properties of specific individual metal centers or from the interactions between heterometallic metal centers thereof. Recent efforts, including from within our group, has specifically explored heterometallic materials containing f-block metals, i.e. the lanthanides and early actinides, with either a d-block metal [8, 12-14] or with another f-block metal,[15-18] with the goal of capturing and harnessing interesting structures with novel properties. A notable example is that from Wang *et al.*, who recently explored the emission of europium incorporated into a uranyl coordination polymer wherein luminescence from both metal centers was observed.[19]

The exploration of 4f-5f bimetallic materials in particular is of interest due to the prevalence of compounds containing both lanthanide and actinide elements in (for example) commercial power and weapons legacy nuclear waste. Both 4f and 5f metal ions exist within UO_2 fuel pellets after irradiation and, as such, one could imagine many situations where metal centers are within close proximity to one another in solution after separations processes and during long-term storage. A few studies have been conducted looking at solid state heterometallic f-element compounds or metal extraction from solution in the context of the separations process involving this mixture of metal ions.[20, 21] Further, despite the perhaps trace amounts of different lanthanides in nuclear fuel, they provide a useful forensics signature for

analysis and geological origins.[22] These situations present an opportunity to study the interactions between, and properties of, different f-elements when they are paired together on a molecular level. Despite sparse examples of 4f-5f materials in the literature, the synthesis of singular compounds[17, 18] and the presentation of systematic studies[23, 24] are becoming more common demonstrating that the synthesis and structural investigation of 4f-5f heterometallic materials is of interest to the broader arena of nuclear fuel stewardship and materials chemistry.

Within such research, our group has focused historically on synthesis and property characterization on hybrid materials containing the uranyl (UO_2^{2+}) unit, the state of uranium most stable in environmentally relevant conditions, in an effort to explore hydrothermal synthesis criteria and subsequent structure-property relationships. [25-27] Synthesis pathways to heterometallic uranyl-containing hybrid compounds are varied and most often utilize multi-functional carboxylate ligands[24, 28, 29] or phosphonates[30, 31] to coordinate multiple, distinct metal centers. The extra functionality provided by multiple coordination sites lends to the formation of coordination polymers of higher dimensionalities (2D sheets and 3D frameworks) while also assisting in the incorporation of secondary metal heteroatoms. These efforts are often necessary due to differences in coordination environments between uranyl and lanthanide metal centers leading to a separation of solid-state phases containing the two metals independently.[24] In this work, however, we do not employ the use of ligands with multiple coordination sites to assemble disparate metal ions through direct bondingand instead utilize the chelating N-donating ligand terpyridine to control the coordination environment of UO_2^{2+} and Ln^{3+} centers and promote non-covalent assembly of relatively similar complexes. Further, the terpyridine and thiophene ligands used herein can perform a sensitizing role (i.e. antenna effect) in energy transfer to metal centers resulting in more efficient luminescent emission.

We report here an isomorphous series of nine new 4f-5f lanthanide-uranyl heterometallic complexes, $\{[(UO_2)_2(O)(L^1)(L^2)_2][UO_2(L^1)_3][Ln(L^1)_3(L^2)] \bullet H_2O\}_2$, and a uranyl only complex, $[(UO_2)_2(O)(L^1)(L^2)_2]_2[UO_2(L^1)_3] \bullet NO_3 \bullet H_2O$, where L^1 and L^2 are 2-thiophenecarboxylic acid ($C_5H_3SO_2$) and 2,2':6'2"-terpyridine ($C_{15}H_{11}N_3$), respectively, and the lanthanides (Ln) used were Pr^{3+} through Er^{3+}, excluding Pm^{3+}. Each complex in the heterometallic series contains three unique molecular building units; two of which feature a uranyl metal center, a monomer and a dimer, and the third features lanthanide metal centers forming a dimer. The uranyl only phase contains *two* crystallograhpically unique uranyl dimers and a single uranyl monomer. The uranyl monomer has a formal charge of -1, the uranyl dimer a formal change of +1, while the lanthanide dimer has a formal change of 0. All of these tectons are held together *via* weak hydrogen interactions and unique offset π-stacking interactions. As the isomorphous series of materials contains two different metal centers, with coordinated antenna ligands, Raman and luminescence spectra were obtained and interesting properties, including simultaneous lanthanide *and* uranyl emission, were observed.

Experimental Section

Materials and Methods

Caution: *Although the uranium used (uranyl acetate dihydrate, ($[UO_2(CH_3COO)_2] \bullet 2H_2O$), and uranyl nitrate hexahydrate, ($[UO_2(NO_3)_2] \bullet 6H_2O$)) in this study is depleted uranium, standard precautions for working with radioactive materials should be followed.*

Lanthanide nitrate salts [$Ln(NO_3)_3 \bullet xH_2O$ (where Ln = Pr^{3+}, Gd^{3+} - Er^{3+}, x = 1, 5, 6, Strem Chemicals, 99.9%), $Nd(NO_3)_3 \bullet 6H_2O$ (Sigma Aldrich, 99.9%), $Ln(NO_3)_3 \bullet 6H_2O$ (where Ln =

Sm^{3+} and Eu^{3+}, Alfa Aesar, 99.9%)] and organic ligands [2,2':6',2"-terpyridine (Strem Chemical, 98%), 2-thiophenecarboxylic acid (Sigma Aldrich, 99%)] are all commercially available and were used as received.

Synthesis

All heterometallic complexes (**1-9**) were synthesized with the same protocols *via* hydrothermal methods. A mixture of uranyl acetate dihydrate, 2,2':6'-2"-terpyridine, 2-thiophenecarboxylic acid, $Ln(NO_3)_3 \bullet xH_2O$ (where Ln = Pr^{3+} - Er^{3+}, x = 1, 5, 6), and 1.5 mL of distilled water (molar ratio approximately 1:1:2:0.5:826) was placed into a 23 mL Teflon lined reaction vessel within a Parr autoclave (masses used provided in Table S13 in the ESI). The pH was adjusted to approximately ~10 with 100 μL of 5M NaOH before the reaction vessels were sealed and heated at 120 °C at autogenous pressure for five days. The autoclaves were allowed to cool to room temperature under ambient conditions over four hours and were opened after approximately sixteen hours. The mother liquor was decanted and the solid reaction product was placed in a petri dish, washed with water and ethanol, and allowed to air-dry at room temperature in a fume hood. The uranyl only phase (**10**) was synthesized when a uranyl nitrate hexahydrate salt was substituted for the uranyl acetate in the synthesis of the U-Tb heterometallic phase, with molar ratios and hydrothermal conditions kept constant (also provided in Table S13 in the ESI). Visual differentiation between the two phases was possible due to shape and color of the single crystals; heterometallic complexes grew as orange-yellow blocks and the uranyl only complex was found as clusters of small yellow plates.

X-ray structure determination

Single crystals of the bulk samples were isolated and mounted on MiTeGen micromounts. Reflection data were collected at 293(2)K (and 100(2)K for **10**) with 0.5° ω and φ scans on a Bruker SMART diffractometer equipped with an APEX II CCD detector using MoKα (λ = 0.71073 Å) radiation. The data were integrated using the SAINT program[32] within the APEX II software suite[33] and an absorption correction was applied using SADABS.[34] Slight non-merohedral twinning in the crystal of complex **10** was ignored due to a less optimized refinement. Complexes **1**, **3 – 5**, **7**, **8**, and **10** were solved *via* direct methods using Superflip[35] and complexes **2**, **6**, and **9** were solved *via* direct methods using SIR 92.[36] All complexes were refined using SHELXL-2014[37] in the WinGX software suite.[38] In each structure, all non-hydrogen atoms were located in difference Fourier maps and were refined anisotropically. Aromatic hydrogen atoms were placed in idealized positions by utilizing the HFIX43 command and allowed to ride on the coordinates of the parent atom with isotropic thermal parameters (U_{iso}) fixed at 1.2 U_{eq}. OMIT 0 0 1 commands were used on all complexes (**1**-**10**) in this study. Additionally, the OMIT 0 1 0 command was utilized in complexes **1**, **7**, and **10** and the OMIT 1 -3 1 and OMIT 1 2 2 commands were used in complex **9**. The 1 0 3, -1 -3 8, -6 -12 14, 1 -7 6, and 9 1 1 OMIT commands were used in complex **10** as well. All OMIT commands were utilized to remove reflections affected by the beamstop. Hydrogen atoms on the lattice water molecules (OW1) in all complexes could not be found in the Fourier map, and were thus not modeled.

Significant thiophene ring disorder is present in all complexes and, as such, PART commands were employed to model the two part ring flipping disorder (TRXA/TRXB, where TR represents "Thiophene ring" and X is the designation given to that ring based upon the

nomenclature of the sulfur atom present, i.e. TR1 is the thiophene ring where S1 (sulfur atom 1) is present). PART commands were applied to all heterometallic complexes for TR1, TR2, TR4, TR6, and TR7 (except for complex **8**, where PART commands were only employed on TR1, TR2, TR6, and TR7). For the uranyl only complex, PART commands were employed on all thiophene rings (TR1 - TR5) as well as to model disorder of a lattice water molecule (OW3), where DFIX commands were also utilized on O-H bonds. All free variable values for complexes **1-9** are presented in Table S1 and for complex **10** in Table S6 in the ESI. Additional SAME, RIGU, and SIMU commands were employed to help restrain the two thiophene ring parts in all complexes. ISOR commands were employed on C77B in **1**, C18B in **2**, C19B in **4**, C38B in **8**, and C76, O5 and O8 in **10**. Structures were checked for additional symmetry using PLATON.[39] All structures were visualized with Mercury[40] and figures were prepared with CrystalMaker.[41] Data collection and refinement details for complexes **1-10** are included in Table 1 (L^1 and L^2 will be used in the place of 2-thiophenecarboxylic acid and 2,2':6'2"-terpyridine, respectively).

Table 1 Crystallographic data for complexes **1-10**

	1	**2**	**3**
Chemical Formula	$\{(UO_2)_2(O)(L^1)(L^2)_2][UO_2(L^1)_3][Pr(L^1)_3(L^2)] \cdot H_2O\}_2$	$\{(UO_2)_2(O)(L^1)(L^2)_2][UO_2(L^1)_3][Nd(L^1)_3(L^2)] \cdot H_2O\}_2$	$\{(UO_2)_2(O)(L^1)(L^2)_2][UO_2(L^1)_3][Sm(L^1)_3(L^2)] \cdot H_2O\}_2$
Formula weight	5145.48	5152.14	5164.36
Crystal system	Triclinic	Triclinic	Triclinic
Space group	$P\bar{1}$	$P\bar{1}$	$P\bar{1}$
a (Å)	10.2461(1)	10.407(8)	10.2491(3)
b (Å)	14.3724(2)	14.594(11)	14.3958(5)
c (Å)	29.2362(4)	29.68(2)	29.1628(10)
α (deg)	81.570(2)	81.683(12)	81.715(1)
β (deg)	88.939(1)	88.909(14)	89.029(2)
γ (deg)	82.321(3)	82.390(11)	82.284(1)
V (Å^3)	4220.64(10)	4420(6)	4219.3(2)
Z	1	1	1
T (K)	293(2)	293(2)	293(2)
λ (Mo Kα)	0.71073	0.71073	0.71073
D_{calc} (Mg cm^{-3})	2.024	1.935	2.032
μ (mm^{-1})	6.557	6.297	6.677
R_{int}	0.0628	0.0378	0.0397
R1 [$I>2\sigma(I)$]	0.0307	0.0314	0.0341

wR2 [$I>2\sigma(I)$]	0.0621	0.0771	0.0717
	4	**5**	**6**
Chemical Formula	$[\{(UO_2)_2(O)(L^1)(L^2)_2][UO_2(L^1)_3][Eu(L^1)_3(L^2)] \cdot H_2O\}_2$	$\{(UO_2)_2(O)(L^1)(L^2)_2][UO_2(L^1)_3][Gd(L^1)_3(L^2)] \cdot H_2O\}_2$	$\{(UO_2)_2(O)(L^1)(L^2)_2][UO_2(L^1)_3][Tb(L^1)_3(L^2)] \cdot H_2O\}_2$
Formula weight	5167.58	5178.16	5181.50
Crystal system	Triclinic	Triclinic	Triclinic
Space group	$P\bar{1}$	$P\bar{1}$	$P\bar{1}$
a (Å)	10.2461(3)	10.2255(3)	10.2340(9)
b (Å)	14.4076(5)	14.4050(3)	14.4042(19)
c (Å)	29.1376(10)	29.0078(7)	29.053(3)
α (deg)	81.788(1)	81.949(1)	81.864(2)
β (deg)	89.038(1)	89.133(3)	89.103(1)
γ (deg)	82.266(1)	82.242(2)	82.241(1)
V (Å^3)	4218.5(2)	4191.93(18)	4200.9(7)
Z	1	1	1
T (K)	293(2)	293(2)	293(2)
λ (Mo Kα)	0.71073	0.71073	0.71073
D_{calc} (Mg cm^{-3})	2.034	2.051	2.048
μ (mm^{-1})	6.726	6.812	6.849
R_{int}	0.0368	0.0503	0.0292
R1 [$I>2\sigma(I)$]	0.0319	0.0313	0.0299
wR2 [$I>2\sigma(I)$]	0.0639	0.0664	0.0665
	7	**8**	**9**
Chemical Formula	$\{(UO_2)_2(O)(L^1)(L^2)_2][UO_2(L^1)_3][Dy(L^1)_3(L^2)] \cdot H_2O\}_2$	$\{(UO_2)_2(O)(L^1)(L^2)_2][UO_2(L^1)_3][Ho(L^1)_3(L^2)] \cdot H_2O\}_2$	$\{(UO_2)_2(O)(L^1)(L^2)_2][UO_2(L^1)_3][Er(L^1)_3(L^2)] \cdot H_2O\}_2$
Formula weight	5188.66	5193.52	5198.18
Crystal system	Triclinic	Triclinic	Triclinic
Space group	$P\bar{1}$	$P\bar{1}$	$P\bar{1}$
a (Å)	10.2216(8)	10.2483(7)	10.2447(3)
b (Å)	14.4037(11)	14.4377(9)	14.4393(5)
c (Å)	29.008(2)	29.0278(19)	29.9870(9)
α (deg)	81.961(2)	81.977(2)	82.023(2)
β (deg)	89.146(1)	89.188(1)	89.223(1)
γ (deg)	82.246(1)	82.246(2)	82.245(2)
V (Å^3)	4190.2(6)	4214.0.(5)	4207.6(2)
Z	1	1	1
T (K)	293(2)	293(2)	293(2)
λ (Mo Kα)	0.71073	0.71073	0.71073
D_{calc} (Mg cm^{-3})	2.056	2.047	2.051
μ (mm^{-1})	6.915	6.928	6.995
R_{int}	0.0471	0.0445	0.0237
R1 [$I>2\sigma(I)$]	0.0317	0.0325	0.0253
wR2 [$I>2\sigma(I)$]	0.0714	0.0632	0.0537
	10		
Chemical Formula	$\{(UO_2)_2(O)(L^1)(L^2)_2]_2[UO_2(L1)_3] \cdot NO_3 \cdot H_2O$		
Formula weight	3028.91		
Crystal system	Triclinic		

Space group	$P\bar{1}$
a (Å)	10.668(2)
b (Å)	20.152(4)
c (Å)	23.297(5)
α (deg)	109.308(3)
β (deg)	101.972(3)
γ (deg)	93.617(3)
V (Å^3)	4576.8(16)
Z	2
T (K)	100(2)
λ (Mo Kα)	0.71073
D_{calc} (Mg cm^{-3})	2.225
μ (mm^{-1})	9.017
R_{int}	0.0644
R1 [I>2σ(I)]	0.0824
wR2 [I>2σ(I)]	0.2082

Powder X-ray diffraction

Powder X-ray diffraction (PXRD) data on the bulk reaction product from each sample were collected on a Rigaku Miniflex (Cu Kα 2θ = 3-60) and were analyzed using the Match! software program.[42] The PXRD patterns of the bulk products of complexes **1-10** were used to check reproducibility and purity and are provided in the ESI section (Fig. S1 - S9 for **1-9**, S25 for **10**). The bulk products of all complexes were found to be impure and consist of a mixture of the U-Ln (or U only) title complexes as well as dimeric lanthanide phases which have been recently reported by Knope *et al*.[43] Visual inspection of reaction products reveals that the overall yields of title complexes were rather low, as all syntheses produced only a few single crystals of each complex per reaction. The yields of the lanthanide only complexes were slightly higher, upon visual inspection, yet only a few single crystals were identified. Further, an unknown amorphous impurity was apparent upon visual inspection.

Luminescence

Visible solid-state luminescence measurements were taken at low temperature (~77K) with a Horiba JobinYvon fluorolog-3 spectrophotometer on complexes **2**, **3**, **4**, **6**, and **7**, containing the Ln^{3+} metal centers Nd^{3+}, Sm^{3+}, Eu^{3+}, Tb^{3+}, and Dy^{3+}, respectively, as well as on the uranyl only phase complex **10**. Data were manipulated using the FluroEssence software package.

Single crystals of the complexes were isolated from the bulk sample and placed into a quartz NMR tube. The tube was then submerged in a vacuum-sealed quartz dewar containing liquid nitrogen for the duration of the spectral data collection. In general, the samples were excited according to the absorption maxima of the 2,2':6',2"-terpyridine (approximately 350 nm) and 2-thiophenecarboxylic acid (approximately 320 nm) as well as to the uranyl center directly (at 420 nm).

Raman Spectroscopy

The Raman spectra of complexes **2**, **3**, **4**, **6**, **7**, and **10** were collected on LabRAM HR Evolution Raman Spectrometer with a 532 nm laser at room temperature. Single crystals of each complex were isolated and placed on a single-welled glass microscope slide with a minimal amount of mineral oil. The Raman spectra are provided in the ESI (Fig. S19-S23, S26 for **10**).

Results

Structural Descriptions

All nine heterometallic complexes crystallize in the triclinic space group $P\bar{1}$ and are isomorphous, the difference between them being the identity of the Ln^{3+} metal center present, and, as such, only complex **4** will be discussed in detail. Complex **4** contains three unique molecular species; a uranyl dimer, a uranyl monomer, and a europium (Eu^{3+}) dimer (Fig. 1). The

asymmetric unit consists of the uranyl monomer, the uranyl dimer, and one half of the Eu^{3+} dimer. The uranyl dimer contains two unique metal centers (U1 and U2), both adopting a pentagonal bipyramid coordination geometry and each chelated by a terpyridine ligand with U-N (N1-N6) bond distances ranging between 2.571(3) Å and 2.634(3) Å (Fig 2). The two uranium metal centers form the dimer *via* a bridging bidentate thiophene ligand, through bond distances of 2.406(3) Å and 2.424(3) Å for U1-O3 and U2-O4, respectively, and a μ-bridging oxide (O5) with bond distances of 2.095(3) Å to U1 and 2.121(2) Å to U2. This dimeric uranyl unit has an overall formal charge of +1 and is charge balanced by the other uranyl unit, a monomer, which has a formal -1 charge. This uranyl monomer is coordinated by three bidentate thiophene ligands to give the metal center a hexagonal bipyramid coordination geometry (Fig. 3). The range of uranium (U3) to thiophene-oxygen bond distances is between 2.450(3) Å and 2.486(3) Å.

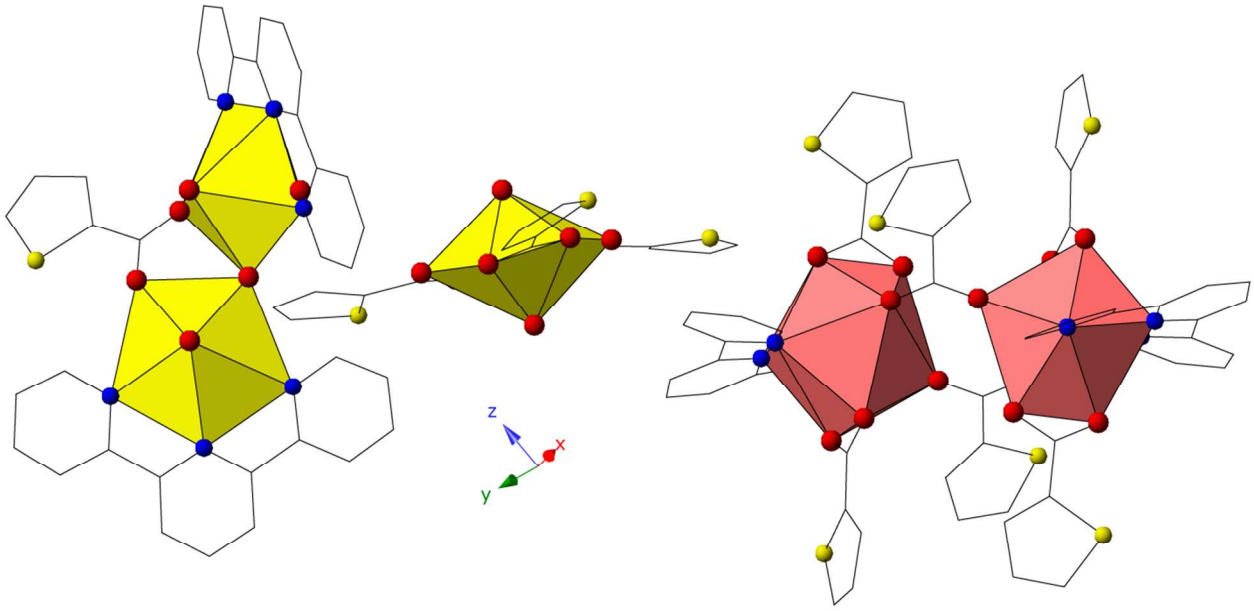

Fig. 1. Polyhedral representation of the three molecular units of complexes**1-9**, where the asymmetric unit consists of the uranyl monomer, the uranyl dimer, and half of the lanthanide dimer, is shown. The left unit is the positively charged uranyl dimer, the middle is the negatively charged uranyl monomer, and the unit on the right is the lanthanide dimer. Yellow and pink polyhedra are uranium and Eu^{3+} metal centers, respectively. Red, blue, and yellow spheres are oxygen, nitrogen, and sulfur atoms, respectively. A lattice water molecule and all hydrogen atoms have been removed for clarity here and throughout the remainder of the manuscript.

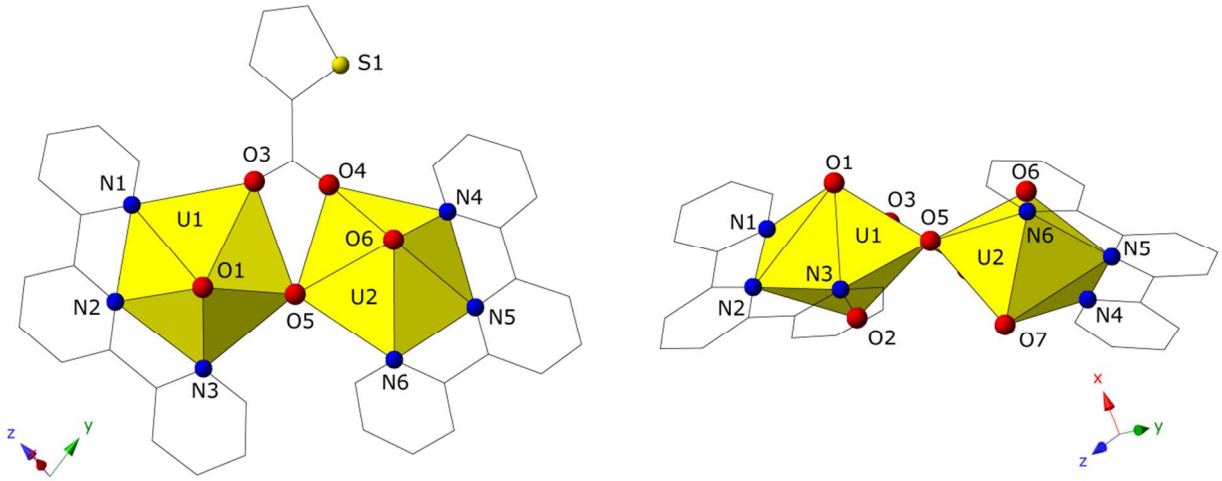

Fig. 2. Two orientations of the positively charged uranyl dimer unit in compounds **1-9**.

The third molecular unit, a Eu^{3+} containing dimer (Fig. 4), has an overall neutral charge and features a single crystallographically unique Eu^{3+} metal center chelated by a TPY ligand at Eu1-N bond distances of 2.580(4), Å 2.628(3) Å, and 2.617(4) Å (Eu1-N7, Eu1-N8, and Eu1-N9, respectively). Further coordination to the Eu^{3+} center occurs with two bidentate thiophene ligands (Eu1-O16: 2.492(3) Å, Eu1-O17: 2.494(3) Å, Eu1-O18: 2.499(3) Å, Eu1-O19: 2.496(3) Å) and a bridging bidentate thiophene ligand which link the symmetry equivalent Eu^{3+} centers together through bond distances of 2.361(3) Å (Eu1-O20) and 2.321(3) Å (Eu1-O21) to form the dimer. The Eu^{3+} metal centers have a coordination number of nine, adopt a distorted tricapped trigonal prismatic geometry, and are separated by a distance of 5.3532(2) Å within a single dimer. Additionally, there is a partially occupied water molecule in the lattice which hydrogen bonds to the carboxylate oxygens O17 and O18 on the two symmetrically unique bidentate thiophene ligands of the Eu^{3+} containing dimer.

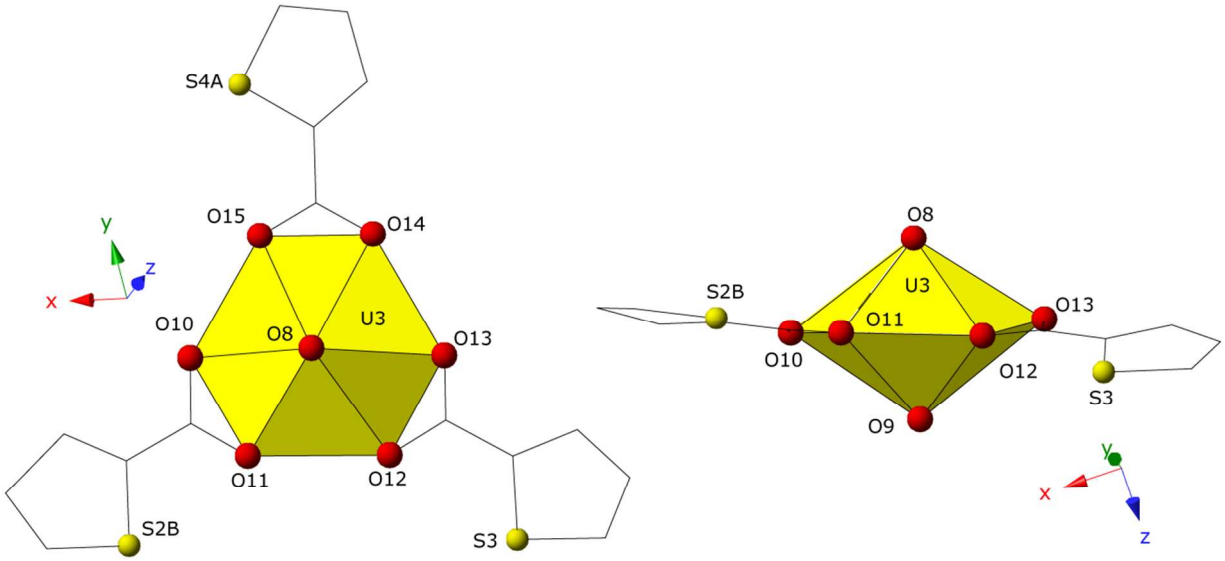

Fig. 3. Two orientations of the negatively charged uranyl monomer unit in compounds **1**-**9**.

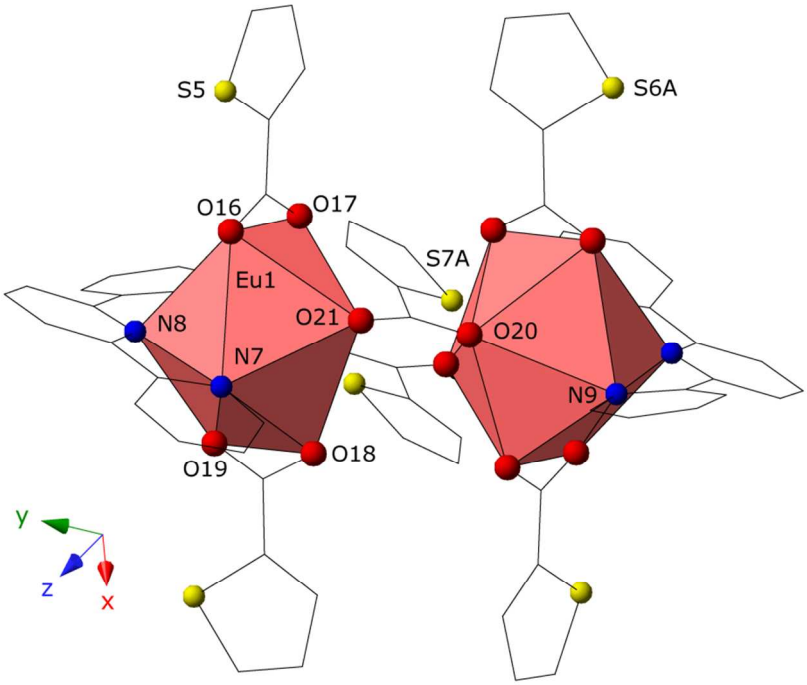

Fig. 4. Polyhedral representation of the Eu^{3+} dimer unit in compound **4**.

The three units are assembled together through several weak hydrogen interactions and a single unique offset π-stacking interaction,[44] between a thiophene ring and the central ring of a terpyridine ligand. This interaction is recreated through inversion symmetry and assembles two uranyl monomers and the europium dimer into a discrete supramolecular entity (Fig. 5). Relevant

distances and angles associated with that interaction are as follows: Cg ··· Cg 3.7049(1) Å, Cg⊥ ··· Cg⊥ Å 3.6276, β = 11.7°. The packing and global structure of complex **4** is shown in Figure 6.

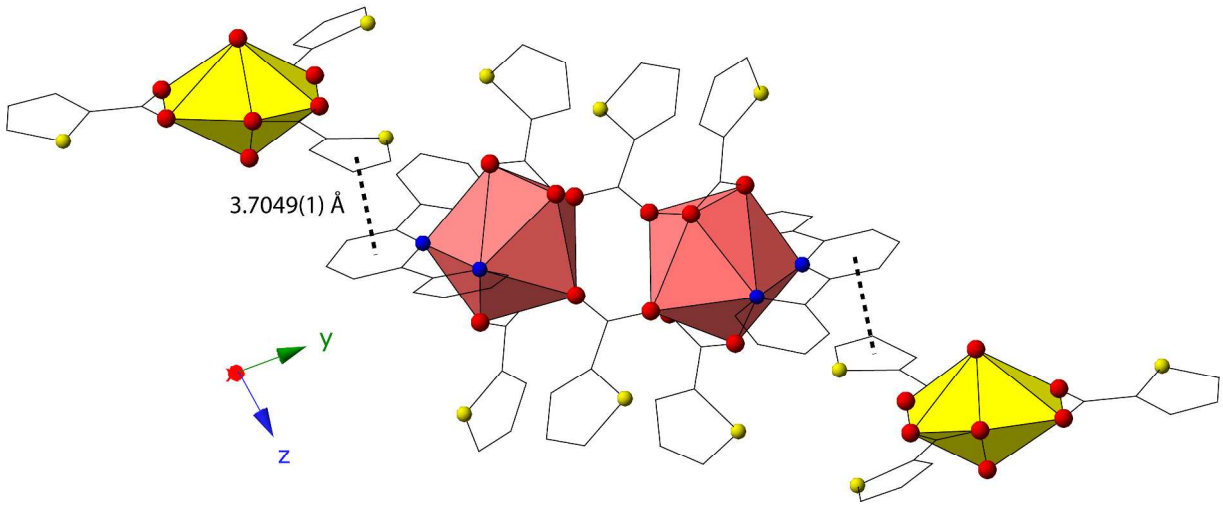

Fig. 5. A europium dimer participating in two offset π-stacking interactions (a single unique interaction) with two uranyl monomers is shown.

Complex **10** (crystallize in $P\bar{1}$) is unlike the other nine materials as it does not incorporate a lanthanide moiety and instead contains two crystallograhpically unique dimers and a uranyl monomer (Fig. 7) which are structurally similar to those observed in the heterometallic complexes. As the individual uranyl molecular units are the same, only the supramolecular assembly will be examined in detail (selected bond distances in Table S7). As with the U-Ln materials, weak hydrogen interactions dominate the assembly of these materials with the exception of three offset π-stacking interactions that work in concert to assemble the two unique uranyl dimers into a 1D chain by involving all four unique terpyridine ligands (ESI Fig. S24). Relevant distances and angles are given here: Cg4 ··· Cg12 3.5581(8) Å, Cg⊥ ··· Cg⊥ Å 3.3248, β = 20.9°, Cg6 ··· Cg14 3.6304(9) Å, Cg⊥ ··· Cg⊥ Å 3.5343, β = 13.2°, Cg7 ··· Cg15 3.5802(8)

Å, Cg⊥ ··· Cg⊥ Å 3.4646, β = 14.6°. Further, lattice water and nitrate molecules are observed in this complex, charge-balancing the uranyl building units.

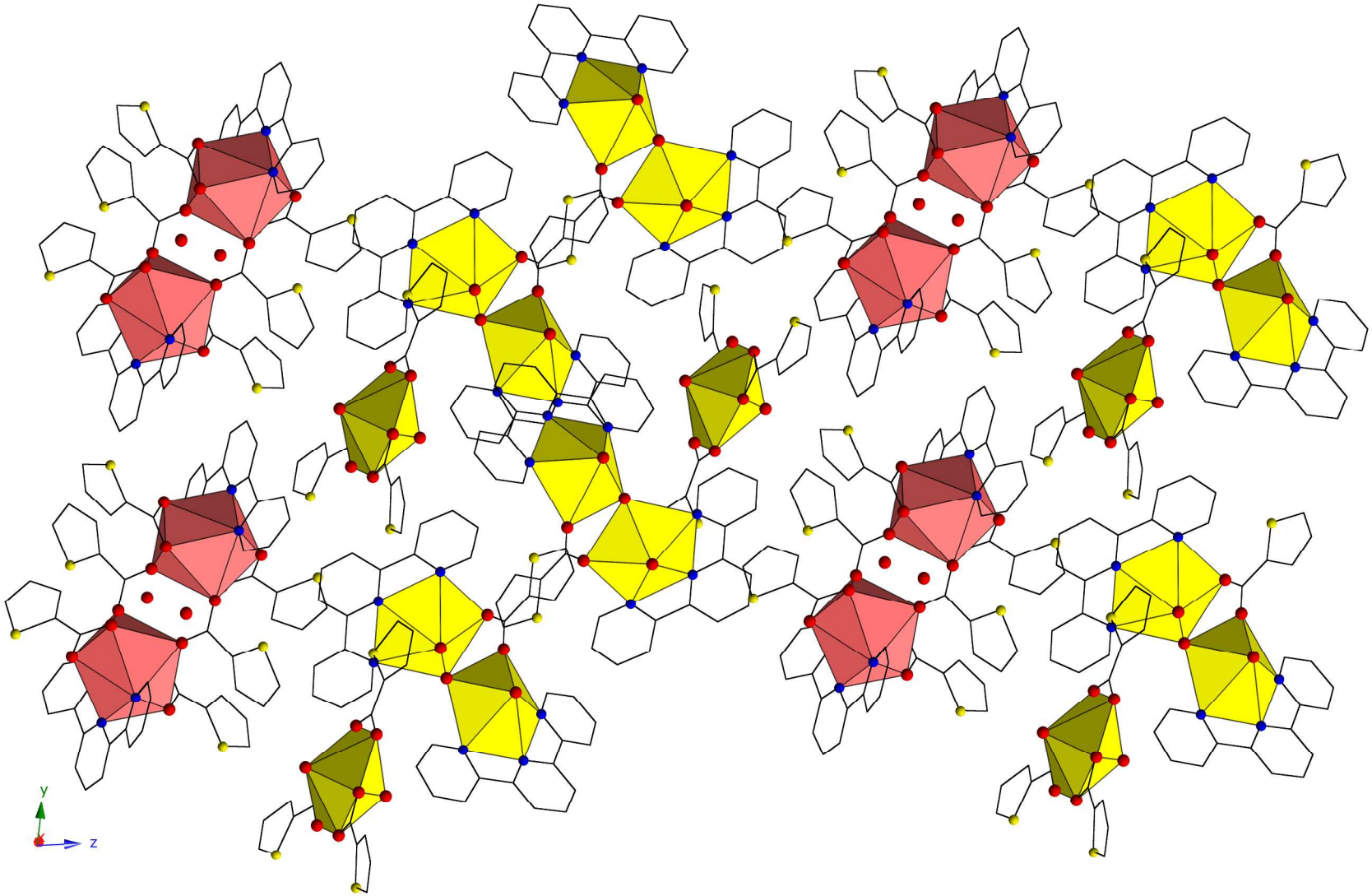

Fig. 6. The global structure of complex **4** is shown. The building units repeat along roughly the z-axis from left to right as: Eu^{3+} dimer, uranyl monomer, uranyl dimer, uranyl dimer, uranyl monomer, Eu^{3+} dimer. Tectons are held together *via* weak hydrogen interactions and two offset π-stacking interactions (one unique).

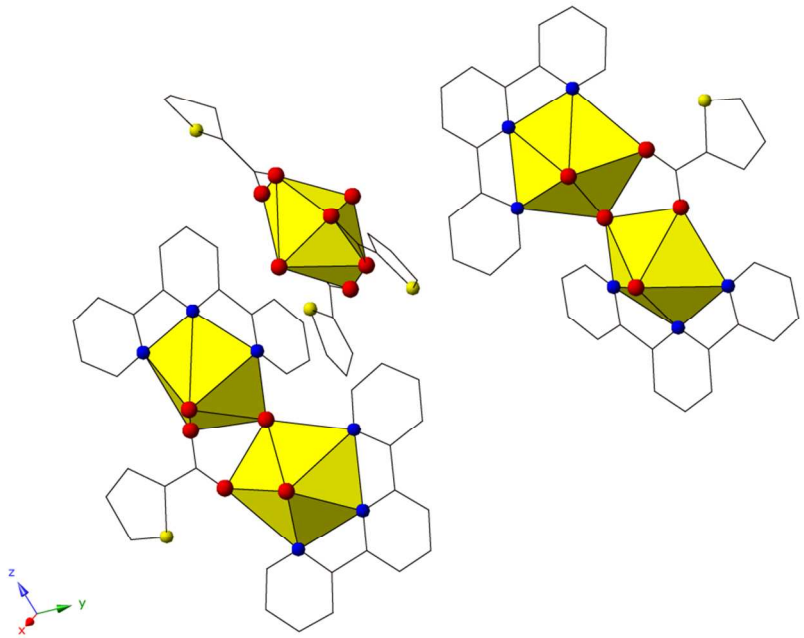

Fig. 7. The asymmetric unit of complex **10** containing two unique uranyl dimers and a uranyl monomer. A lattice water molecule and disordered lattice nitrate were removed for clarity.

Discussion

Structural Discussion

The complexes presented herein provide an interesting opportunity to explore the first coordination spheres within eachand compare them to similar moieties in the literature. The synthesis and characterization of hybrid materials containing N-donors with the lanthanides[25, 45-48] and the uranyl[12, 49-51] has been explored significantly in our group over the past few years, helping to provide context to discuss coordination motifs for a comparative structural analysis.

Starting with the most simple of the units, the uranyl monomer contains a single uranyl unit coordinated by three bidentate thiophene ligands producing a hexagonal bipyramid coordination environment. This monomeric uranyl motif with three bidentate carboxylates is rather common in the literature and occurs in 105 unique uranyl structures in the CSD (V5.38, May 2017).[52-55] This tri-carboxylato coordination is also common in coordination polymers (CPs) of varying dimensionality, appearing in 35 structures.[56, 57] Our group has also observed

this uranyl-carboxylate motif in molecular uranyl compounds recently within a series of heterometallic complexes.[58] The more complex uranyl dimer contains two unique uranyl centers, both coordinated by terpyridine ligands, and bridged by an oxide and a thiophene ligand. Despite the use of terpyridine as a capping ligand in multiple uranyl studies, we have not synthesized compounds that have this dimeric, double terpyridine motif.[49, 50, 59] To our knowledge, the only uranyl material that shares a close coordination environment is that of a terpyridine containing uranyl dimer with dicyanoaurate published recently.[60]

The lanthanide dimer perhaps allows for the most interesting in depth discussion and comparisons related to the first coordination sphere, as our group[45-47] and others[43] have synthesized complexes that are structurally similar. The lanthanide moiety presented herein contains two symmetry equivalent metal centers with two chelating terpyridine ligands, four bidentate and two bridging bidentate thiophene ligands. As mentioned previously, a lanthanide only phase, recently reported by Knope *et al.* as "structure type II", crystallizes along with the title complexes.[43] This dimer consists of two symmetry equivalent metal centers, two terpyridines, two bidentate, two bridging bidentate and two monodentate thiophene ligands and a coordinated water molecule, marginally different to the one observed in the heterometallic complexes presented herein.[43] The lanthanide contraction can produce slight changes to the coordination environment around lanthanide ions,[45] yet we observe differences between these two lanthanide moieties despite the use of the same metal centers (e.g. Eu^{3+}). Further, as the Ln^{3+} ionic radii in the materials published by Knope, et. al get smaller (toward Ho^{3+} and Er^{3+}), coordination environments change significantly to asymmetric dimers and monomers, variation which are not apparent in the U-Ho and U-Er materials herein. The appearance of a single

lanthanide coordination moiety across all complexes herein is, perhaps, due to influence and interactions originating from the neighboring uranyl tectons.

Luminescence Studies

The luminescent emission spectra of complexes **2**, **3**, **4**, **6**, **7**, and **10** were collected at liquid nitrogen temperature by exciting at several different wavelengths associated with the uranyl absorption band (around 420 nm) and the two organic ligands capable of sensitizing metal based emission, thiophene (around 320 nm) and terpyridine (around 350 nm). Both terpyridine[61, 62] and ligands containing thiophene substituents[51, 63-65] are known organic chromophores with triplet energy levels at appropriate energies (around 22,624 cm^{-1} [62] and 28,388 cm^{-1},[65] respectively, and approximately 2000 – 5000 cm^{-1} above emissive excited states) to facilitate efficient metal center sensitization in lanthanides *via* the antenna effect.[66, 67] There is also evidence that the uranyl can be sensitized in a similar way,[68] though ascertaining the role or amount of sensitization is difficult as the ligands used herein, and many other organic antenna ligands, have absorption bands in the same region as the uranyl itself.[51] We can, though, surmise that there are several potential emissive energy pathways within this molecular system as both the uranyl and the lanthanide metal centers are coordinated by thiophene and terpyridine ligands. Possible pathways include; thiophene to UO_2^{2+} and Ln^{3+}, terpyridine to UO_2^{2+} and Ln^{3+}, and possibly energy transfer between UO_2^{2+} and Ln^{3+} metal centers. Further, as multiple metal centers are present in each heterometallic compound (i.e. UO_2^{2+} and Ln^{3+}), emission from multiple building units might be expected when exciting at wavelengths associated with coordinated ligands. As such, the five bimetallic complexes mentioned above were analyzed for their ability to display

luminescent emission from different metal centers selectively, observing just uranyl *or* lanthanide emission, or cooperatively, observing both uranyl *and* lanthanide emission.

Uranyl emission originates from vibronic coupling of a ligand-to-metal charge transfer transitions between uranyl bonding ($3\sigma_u$, $3\sigma_g$, $2\pi_u$, and $1\pi_g$) and non-bonding ($5f\delta_u$ and φ_u) molecular orbitals with a Raman-active vibrational mode.[69, 70] Typically, this manifests as four to six vibronic peaks in the 400-650 nm range and results in the green emission characteristic of luminescent uranyl materials. Alternatively, lanthanide emission arises from Laporte forbidden f-f electronic transitions following direct excitation of core-like 4f electrons,[71] yet as mentioned previously an antenna chromophore ligand can enhance this inefficient luminescence.[72]

Excitation of complex **2** (Nd^{3+}) at 350 nm, 420 nm, and 492 nm produces similar intensity vibronic progressions between 500 nm and 625 nm with major peaks at 525 nm, 549 nm, 575 nm, and 604 nm (Fig. 8). Less intense peaks (found at 540 nm, 567 nm, and 592 nm) are also observed in between the major vibronic peaks of all complexes presented (except for the Tb complex **6**), the possible origins of which could be associated with a second emissive uranyl entity, as there are multiple uranyl units in the complex. This possibility will be discussed in greater detail later within the context of other heterometallic complexes and complex **10**. As Nd^{3+} is a near-IR emitter, complex **2** was analyzed in the near-infrared, at several excitation wavelengths, for emission from the lanthanide metal center. No NIR emission was observed, even with the use of antenna ligands, which may be indicative of poor sensitization *via* inefficient energy pathways, non-radiative deactivation the Nd^{3+} emissive excited states, or a combination of both factors.

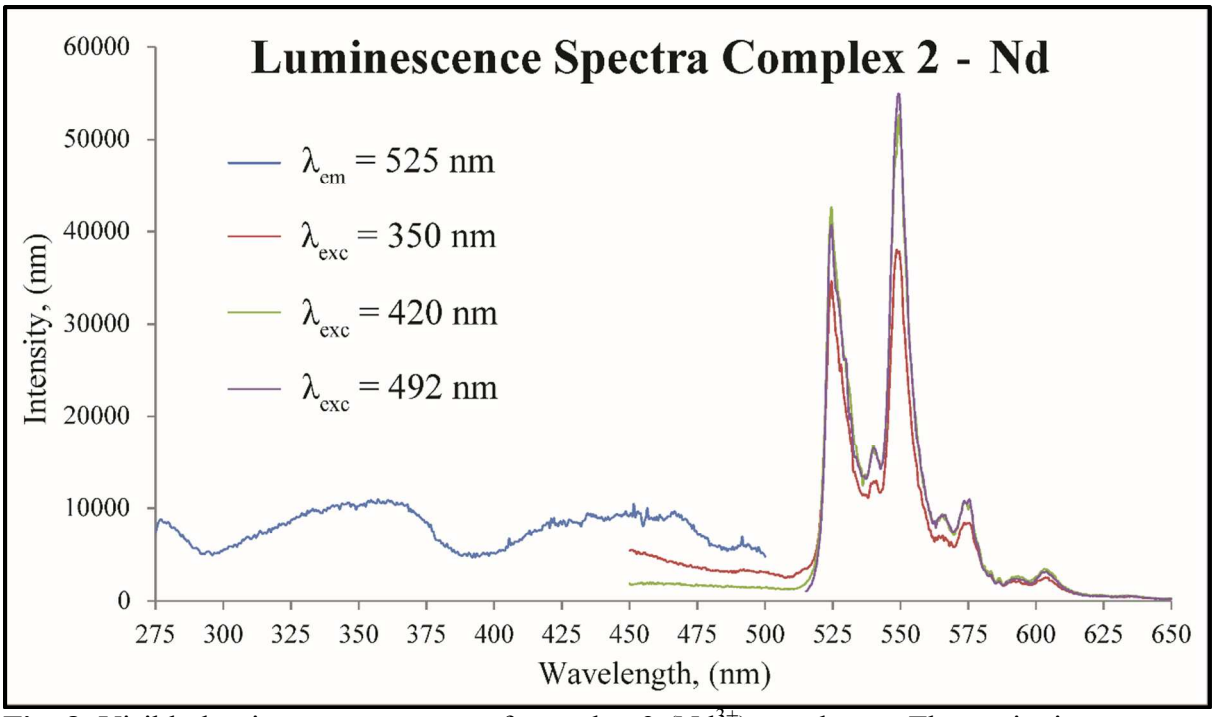

Fig. 8. Visible luminescence spectra of complex **2** (Nd^{3+}) are shown. The excitation spectrum is the blue line, and the red, green, and purple lines are emission spectra collected when exciting at wavelengths of 350 nm, 420 nm, and 492 nm, respectively.

Almost identical uranyl luminescence is observed with complex **3** (Sm^{3+}) (Fig. 9) when exciting at 358 nm and 420 nm, with peaks at 525 nm, 549 nm, 576 nm, and 604 nm, and with complex **7** (Dy^{3+}) (Fig. 10) when exciting at 320 nm, 350 nm, and 420 nm (observed peaks at at 525 nm, 549 nm, 576 nm, and 603 nm). In both of these complexes, we see spectra with similar emission intensity when exciting at different wavelengths, such as in complex **7** when exciting at 320 nm and 350 nm. Yet, again, we observe no obvious lanthanide emission from Sm^{3+} and Dy^{3+}.

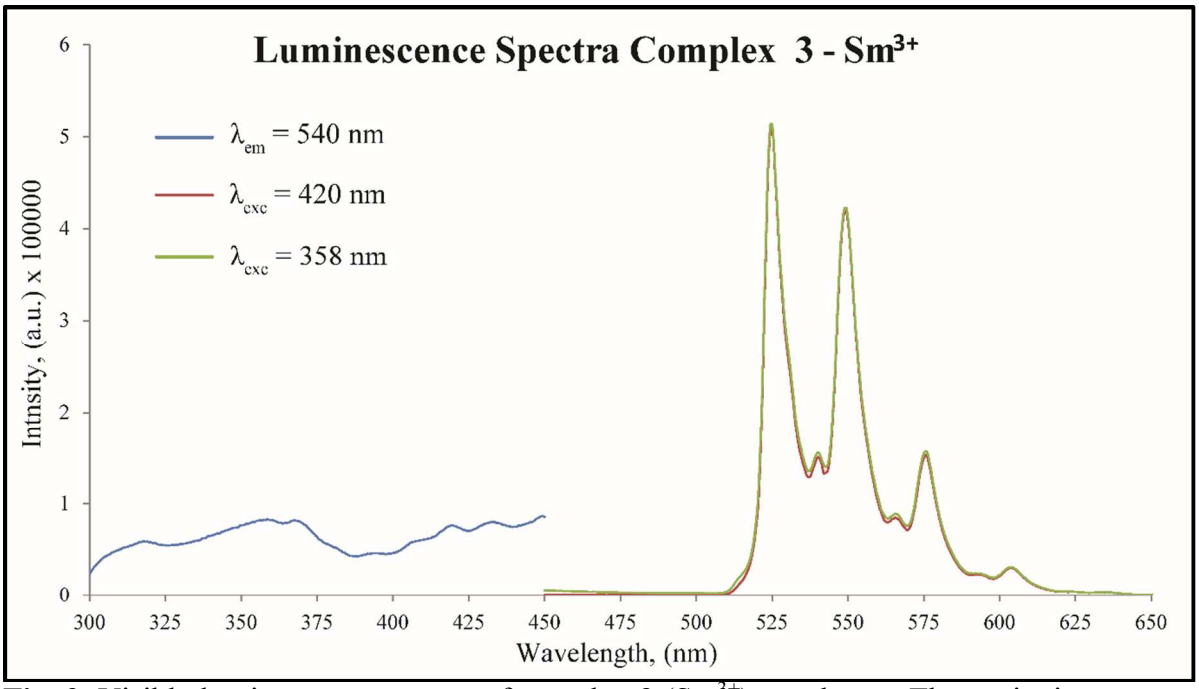

Fig. 9. Visible luminescence spectra of complex **3** (Sm^{3+}) are shown. The excitation spectrum is the blue line, and the green and red lines are emission spectra collected when exciting at wavelengths of 358 nm and 420 nm, respectively.

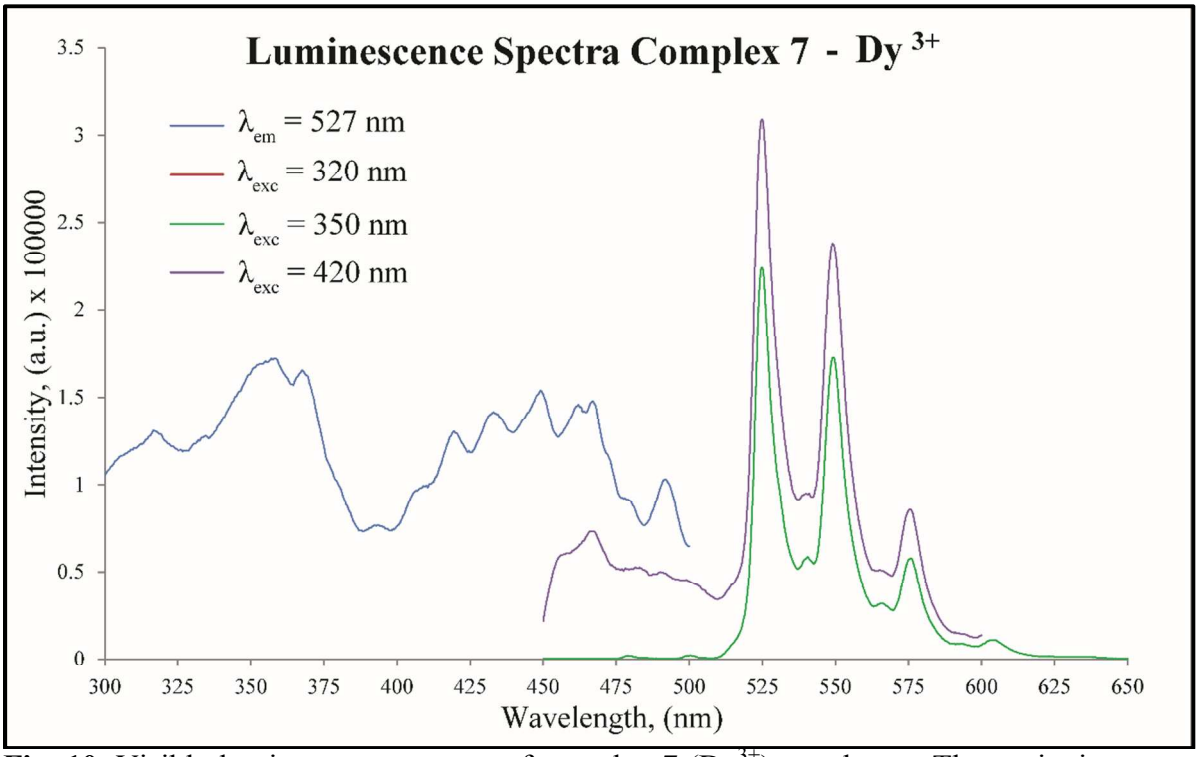

Fig. 10. Visible luminescence spectra of complex **7** (Dy^{3+}) are shown. The excitation spectra is the blue line, and the purple, red, and green lines are emission spectra collected when exciting at wavelengths of 320 nm, 350 nm, and 420 nm, respectively. Purple and red lines are overlaying due to similarity of emission intensity.

Typical uranyl emission in complex **4** (Eu^{3+}) is observed as the major emissive entity at all excitation wavelengths analyzed (328 nm, 394 nm, and 420 nm) with emission peaks observed at 525 nm, 549 nm, 576 nm, and 604 nm (Fig. 11). Unlike the previously discussed UO_2^{2+}-Ln^{3+} compounds, however, excitation with incident light at several wavelengths produces emission from both the uranyl and the europium metal centers concurrently, and only specific wavelengths generate significantly intense Eu^{3+} emission. Luminescence from the Eu^{3+} center is observed as split peaks at 593 nm (589 nm) and 617 nm (614 nm), corresponding to the $^5D_0 \rightarrow {}^7F_1$ and $^5D_0 \rightarrow {}^7F_2$ electronic transitions, respectively, when excited at the absorption maxima of the thiophene ligand (328 nm) or directly exciting the Eu^{3+} with the $^5L_6 \leftarrow {}^7F_0$ transition (394 nm), which directly populates the 4f levels.[73] Luminescence spectra collected on complex **6** (Tb^{3+}) show a similar phenomenon (Fig. 12), where only uranyl luminescence is observed when exciting at 420 nm (emission peaks at 526 nm, 550 nm, 576 nm, and 604 nm) and both uranyl and Tb^{3+} luminescence when exciting at the thiophene ligand (335 nm). Exciting at that energy produces relatively weak uranyl emission peaks centered at 524 nm, 546 nm, and 575 nm and more intense terbium emission peaks at 488 nm, 543 nm, 584 nm, and 620 nm, which correspond to the $^5D_4 \rightarrow {}^7F_6$, $^5D_4 \rightarrow {}^7F_5$, $^5D_4 \rightarrow {}^7F_4$, and $^5D_4 \rightarrow {}^7F_3$ transitions, respectively. In this way, we can somewhat selectively excite the lanthanide in these complexes to induce specific Ln^{3+} emission, at certain excitation energies, in addition to the uranyl luminescent signature arising from near broadband excitation throughout the UV and blue visible region.

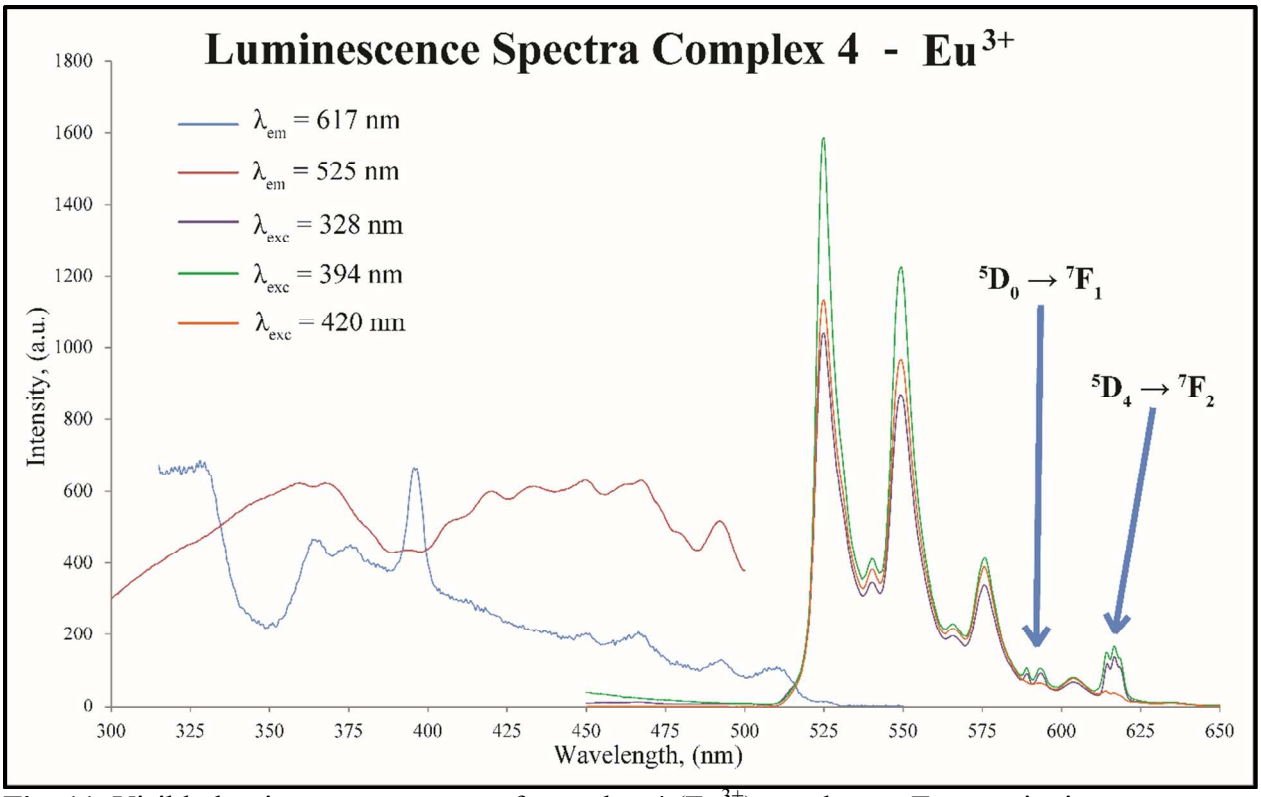

Fig. 11. Visible luminescence spectra of complex **4** (Eu^{3+}) are shown. Two excitation spectra are shown; the blue line is associated with Eu^{3+} emission and the red line is the uranyl. The purple, green, and orange lines are emission spectra collected when exciting at wavelengths of 328 nm, 394 nm, and 420 nm, respectively. The observed Eu^{3+} transitions are labeled. Excitation and emission intensities were normalized to allow more accesible graphical comparisons.

As mentioned previously, less intense emission peaks are observed between a more resolved, higher intensity emission profile in all heterometallic complexes investigated, except for **6**. Several reports observe and discuss this luminescent observation as further coupling of the "yl" bending or ligand vibrational modes with the uranyl excited state, causing additional emission or peak splitting.[70, 74-77] Whereas we acknowledge that this may be the case, we find it more likely that these less intense peaks are associated with another emissive uranyl moiety with a distinct emission profile. The energy of uranyl emission, and thus the peak position in luminescence spectra, is highly dependent on the coordination environment of uranyl metal centers. Weakening or strengthening of the U-O_{yl} bond caused by the electron donating or withdrawing abilities of the equatorially coordinated ligands, respectively,[78] manifest as either

red- or blue-shifts in the vibrational and luminescent spectra.[50] This occurs most notably with oligomerization in uranyl species as a substantial red-shift.[79] As such, we posit that both uranyl species, the monomer and the dimer, are observed in the luminescence spectra and are differentiable due to the red-shift cause by the oligomerization seen in the dimeric species compared to the monomer.

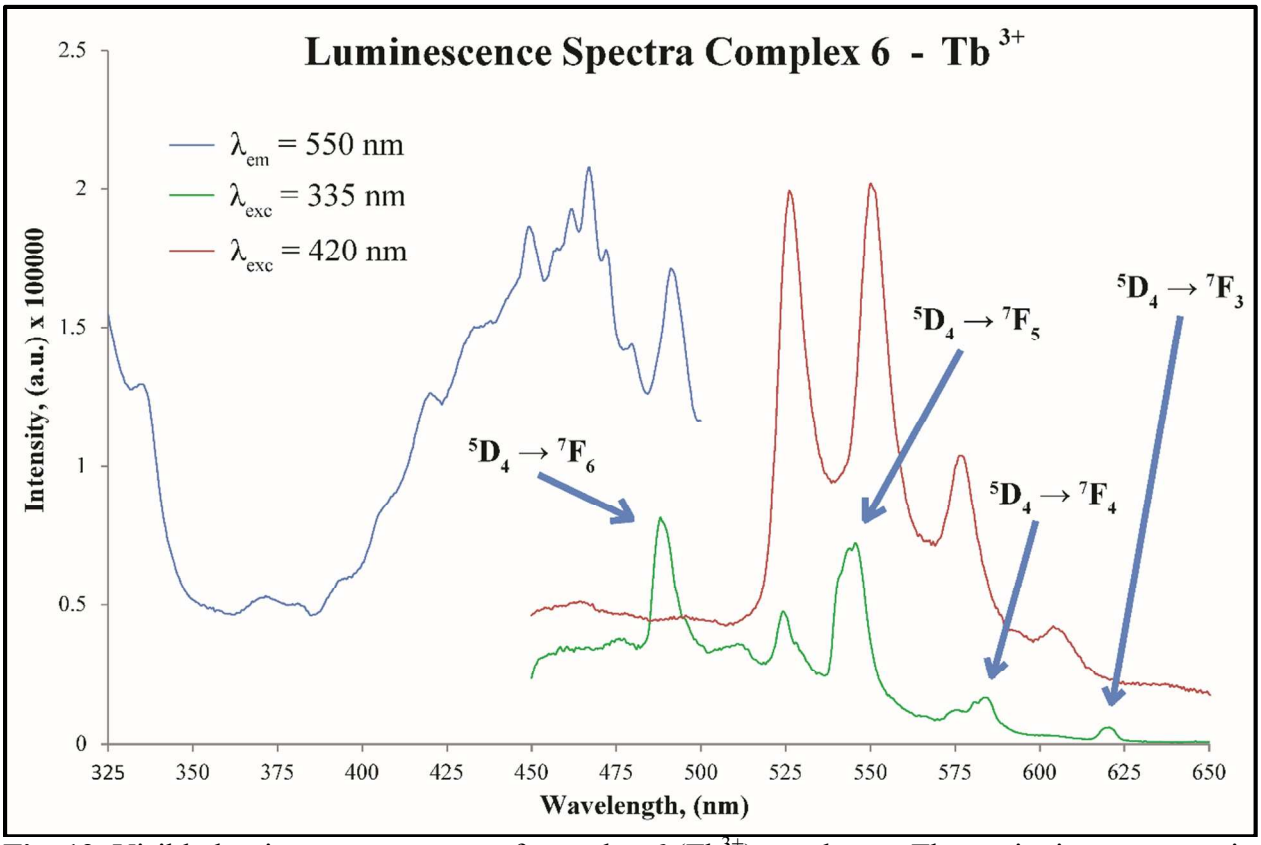

Fig. 12. Visible luminescence spectra of complex **6** (Tb^{3+}) are shown. The excitation spectrum is the blue line. The green and red lines are emission spectra collected when exciting at wavelengths of 335 nm and 420 nm, respectively. The observed Tb^{3+} transitions are labeled.

Definitive ascription of the emission profile for a certain species is difficult, yet a tentative determination is possible. For this, an exploration of the luminescent emission spectra of complex **10** is somewhat helpful (Fig. 13). When excited at 374 nm or 420 nm, a single emission profile is observed (535 nm, 558 nm, 584 nm, and 613 nm) yet, when excited at 335 nm (green), additional slightly less intense peaks appear (at approximately 525 nm, 548 nm, and 575

nm). Interestingly, the peak positions of the more intense uranyl emission profile for the heterometallic complexes are the same energy as those less intense peaks observed in the spectrum of complex **10**, whereas the more intense peaks in **10** correspond to the less intense peaks in the heterometallic materials. (Fig. 14) This suggests that the most intensely emitting uranyl species in the U-Ln complexes and the uranyl only complexes are different, perhaps due to the appearance of an additional dimer in complex **10**. A tentative assignment of the major emissive profiles observed in the U-Ln and U only (with peaks at 525 nm and 535 nm, respectively) materials are that they originate from the monomeric and dimeric units, respectively. This determination is informed by the comparative red-shifting of one emission profile, which follows expected uranyl spectroscopic trends, and that the luminescent signature at 535 nm is more intensely emitting (compared to the other uranyl profile at 525) in the complex with a higher concentration of the dimeric species (2:1 in **10** as opposed to 1:1 in **1-9**).

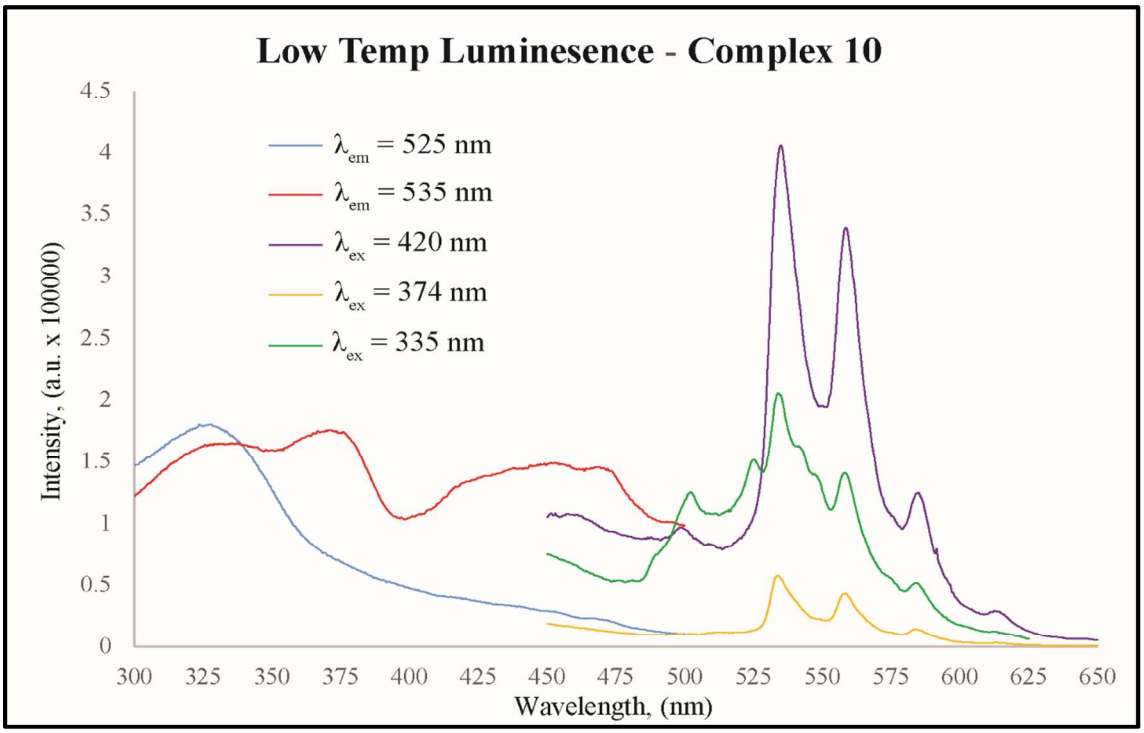

Fig. 13. Visible luminescence spectra of complex **10** (Uranyl only) are shown. Excitation spectra are in blue and red line. The green, yellow, and purple lines are emission spectra collected when exciting at wavelengths of 335 nm, 374 nm, and 420 nm, respectively. A single emission profile

is apparent when excited at 374 nm and 420 nm, but two superimposed emission profiles are observed when excited at 335 nm.

Additionally, the uranyl has been shown to sensitize certain lanthanide centers in glasses or in sol-gels, as compiled by Binnemans,[66] yet within all of these compounds we see no definitive evidence of lanthanide excitation *via* the uranyl. This mostly likely has to do with the proximity of the uranyl and lanthanide metal centers, all of which are in the range of 8 to 12 Å apart, or absences of direct energy pathways. The concurrent emission of the uranyl and a lanthanide is most likely a factor of overlapping absorption bands associated with the metal centers and/or the ligands. As mentioned previously, emission from the uranyl is associated with a wide range of excitation wavelengths, from the UV to the blue visible, encompassing the absorption bands of the uranyl and coordinated ligands, whereas the lanthanide is excited at only very specific energies related to appropriate antenna ligands (like the thiophene in the case of complex **6**) or with the very specific f-orbital transitions (such as in the case of complex **4**).

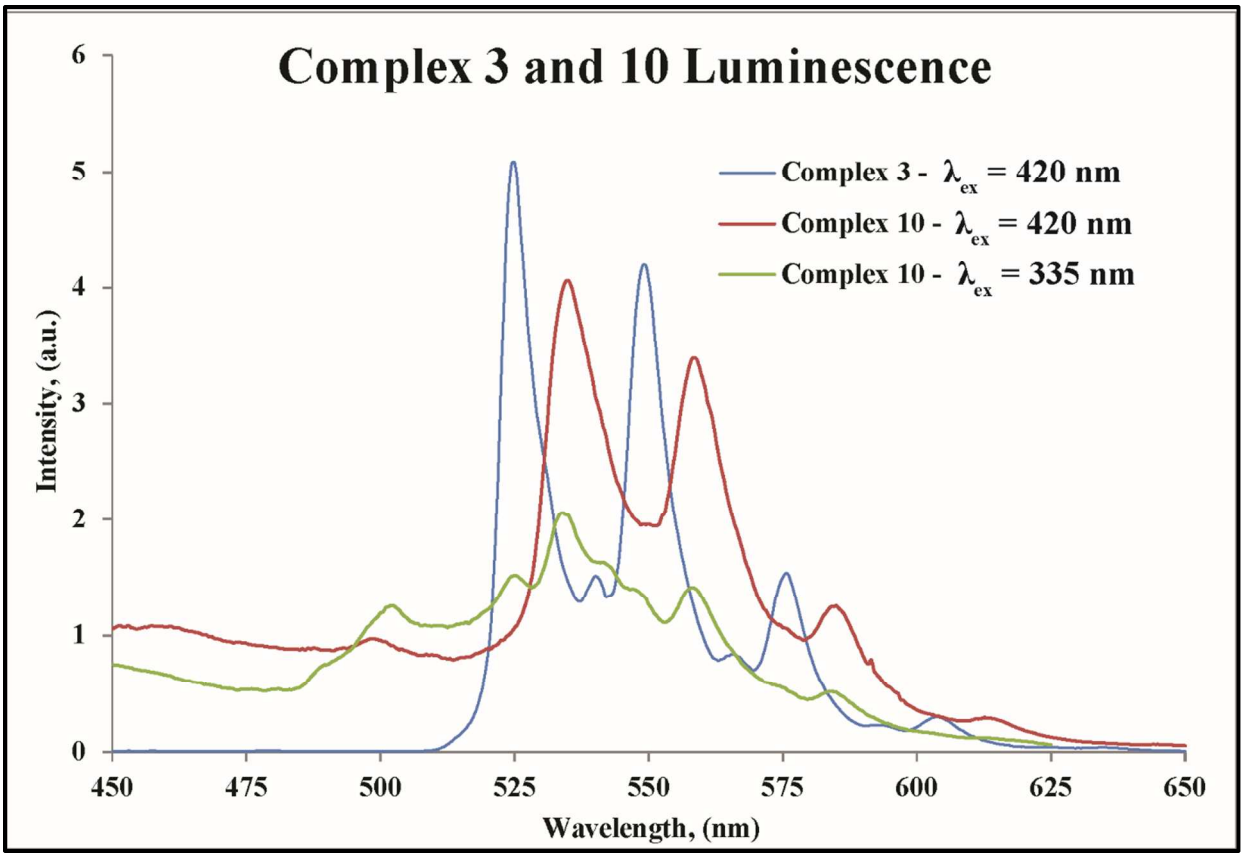

Fig. 14. Visible luminescence spectra of complex **3** and **10** are shown. The blue line corresponds to the luminescent spectra of **3** when excited at 420 nm. The red and green lines are emission spectra collected when exciting at 420 nm and 335 nm, respectively. These overlaid spectra show the difference in the most intense emissive profile for the two complexes.

Raman Analysis

In addition to luminescence measurements, complexes **2**, **3**, **4**, **6**, **7**, and **10** have been characterized using Raman spectroscopy. The linear triatomic uranyl unit (O=U=O) has three distinct normal vibrational modes, one of which is the Raman-active symmetric stretch (ν_1).[80, 81] This Raman stretch is generally observed between 800 and 880 cm^{-1},[82-84] (around 880 cm^{-1} in an aqueous solution) and coordination of ligands to the equatorial plane of the uranyl unit can decrease that value significantly.[79, 85, 86] In all the complexes mentioned above, two peaks are observed in this region which could be associated with the raman-active ν_1 stretch, at 814 cm^{-1} and 849 cm^{-1}. As there are multiple unique uranyl metal centers within these complexes, we

suggest that both observed peaks correspond to the two different uranyl units, the uranyl dimer and monomer, respectively. These assignments are informed by a consensus that oligomerized uranyl species have symmetric stretches which are significantly red-shifted compared to the free ion in solution and non-oligomerized species.[83, 85, 87-89] Further, additional peaks are observed around 797 cm^{-1}, 830 cm^{-1}, and 861 cm^{-1} in the more resolved raman spectra obtained, yet we hesitate to comment on their assignment. Interestingly, only one defined peak is observed for complex **10**, at 809 cm^{-1} despite five unique uranyl metal centers. This observation is of note and appears to contradict our comments on assignment above. Certainly a more in depth treatment (including computational efforts) is warranted and is currently underway.

Conclusions

The synthesis and structure of nine new lanthanide-uranyl 4f-5f bimetallic complexes and a uranyl only phase containing 2-thiophenecarboxlic acid and 2,2';6',2"-terpyridine are reported. Interesting comparisons have been made between the title complexes herein and other materials in recent literature, alluding to structural influences on the lanthanide moieties by the uranyl species. Raman and luminescence spectroscopic analyses were conducted on five of the nine complexes which contain lanthanide metal centers that emit in the visible and near-IR ranges. Two of these five complexes, featuring Eu^{3+} and Tb^{3+} metal centers, show well-defined, concurrent, and selective lanthanide emission following specific excitation associated with antenna ligands and Ln^{3+} transitions superimposed upon the characteristic emission series of the uranyl vibronic bands. Raman spectra of analyzed heterometallic complexes show two large peaks corresponding to the uranyl symmetric stretches from both uranyl tectons, the monomer

and the dimer. In depth spectroscopic and computational studies are necessary for exploration of energy transfer pathways within these very complex f-f bimetallic systems.

Notes

The authors declare no conflicts of interest.

Electronic supplementary information (ESI) available: PXRD patterns of all complexes, ORTEP figures of all complexes, tables of selected bond distances, and other additional information. CCDC: 1843696-1843705. For ESI and crystallographic data in CIF or other electronic format see DOI:

Acknowledgements

This material is based on work supported as part of the Materials Science of Actinides, an Energy Frontier Research Center funded by the U.S. Department of energy, Office of Science, Office of Basic Energy Sciences, under Award Number DE-SC0001089. The authors would like to thank Ms. Alyssa Adcock at Georgetown University for assistance and the use of their LabRAM HR Evolution Raman Spectrometer. JAR and CLC also extends special thanks to Dr. Simon J. A. Pope at Cardiff University for helpful discussions on time-resolved emission measurements and to Dr. Ray J. Butcher at Howard University for crystallographic discussions.

References

1. S. E. Watkins, D. C. Craig and S. B. Colbran, *J. Chem. Soc., Dalton Trans.*, 2002, 2423-2436.
2. F. Scalambra, M. Serrano-Ruiz and A. Romerosa, *Macromol. Rapid Commun.*, 2015, **36**, 680-693.

3. P. Buchwalter, J. Rosé and P. Braunstein, *Chem. Rev.*, 2015, **115**, 28-126.
4. L.-D. Lin, X.-X. Li, Y.-J. Qi, X. Ma and S.-T. Zheng, *Inorg. Chem.*, 2017, **56**, 4635-4642.
5. Y.-Q. Sun, Q. Liu, L.-L. Zhou and Y. P. Chen, *CrystEngComm*, 2014, **16**, 3986-3993.
6. A. S. Jayasinghe, M. K. Payne and T. Z. Forbes, *J. Sol. State Chem.*, 2017, **254**, 25-31.
7. W. Chen, H.-M. Yuan, J.-Y. Wang, Z.-Y. Liu, J.-J. Xu, M. Yang and J.-S. Chen, *J. Am. Chem. Soc.*, 2003, **125**, 9266-9267.
8. K.-X. Wang and J.-S. Chen, *Acc. Chem. Res.*, 2011, **44**, 531-540.
9. D. Guo, C.-Y. Duan, F. Lu, Y. Hasegawa, Q.-J. Meng and S. Yanagida, *Chem. Commun.*, 2004, 1486-1487.
10. B. Zhao, X.-Y. Chen, P. Cheng, D.-Z. Liao, S.-P. Yan and Z.-H. Jiang, *J. Am. Chem. Soc.*, 2004, **126**, 15394-15395.
11. J.-L. Liu, J.-Y. Wu, C. Y.-C., V. Mereacre, A. K. Powell, L. Ungur, L. F. Chibotaru, X.-M. Chen and M.-L. Tong, *Angew. Chem Int. Ed.*, 2014, **53**, 12966-12970.
12. P. Thuery and J. Harrowfield, *Dalton Trans.*, 2017, **46**, 13660-13667.
13. Z. Weng, Z.-H. Zhang, T. Olds, M. Sterniczuk and P. C. Burns, *Inorg. Chem.*, 2014, **53**, 7993-7998.
14. J. A. Ridenour, M. M. Pyrch, Z. J. Manning, J. A. Bertke and C. L. Cahill, *Acta Cryst. C*, 2017, **C73**.
15. K. E. Knope, D. T. de Lill, C. E. Rowland, P. M. Cantos, A. de Bettencourt-Dias and C. L. Cahill, *Inorg. Chem.*, 2012, **51**, 201-206.
16. E. J. Schelter, J. M. Veauthier, J. D. Thompson, B. L. Scott, K. D. John, D. E. Morris and J. L. Kiplinger, *J. Am. Chem. Soc.*, 2006, **128**, 2198-2199.
17. C. Volkringer, N. Henry, S. Grandjean and T. Loiseau, *J. Am. Chem. Soc.*, 2012, **134**, 1275-1283.
18. P. Thuéry and J. Harrowfield, *Cryst. Growth Des.*, 2014, **14**, 4214-4225.
19. J. Xie, Y. Wang, M. A. Silver, W. Liu, T. Duan, X. Yin, L. Chen, J. Diwu, Z. Chai and S. Wang, *Inorg. Chem.*, 2018, **57**, 575-582.
20. V. A. Babain, M. Y. Alyapyshev and R. N. Kiseleva, *Radiochem. Acta*, 2006, **95**, 217-223.
21. B. Chapelet-Arab, G. Nowogrocki, F. Abraham and S. Grandjean, *J. Solid State Chem.*, 2005, **178**, 3046-3054.
22. E. Keegan, M. J. Kristo, K. Toole, R. Kips and E. Young, *Anal. Chem.*, 2016, **88**, 1496-1505.
23. Y.-N. Hou, X.-T. Xu, N. Xing, F.-Y. Bai, S.-B. Duan, Q. Sun, S.-Y. Wei, Z. Shi, H.-Z. Zhang and Y.-H. Xing, *ChemPlusChem*, 2014, **79**, 1304-1315.
24. I. Mihalcea, C. Volkringer, N. Henry and T. Loiseau, *Inorg. Chem.*, 2012, **51**, 9610-9618.
25. K. P. Carter and C. L. Cahill, in *Handbook on the Physics and Chemistry of Rare Earths*, eds. J.-C. G. Bünzli and V. K. Pecharsky, Elsevier, 2015, vol. 47, pp. 147-208.
26. R. G. Surbella and C. L. Cahill, in *Handbook on the Physics and Chemistry of Rare Earths*, eds. J.-C. G. Bünzli and V. K. Pecharsky, Elsevier, 2015, vol. 48, pp. 163-285.
27. C. L. Cahill, D. T. de Lill and M. Frisch, *CrystEngComm*, 2007, **9**, 15-26.
28. P. Thuéry, *Cryst. Growth Des.*, 2014, **14**, 1665-2676.
29. P. Thuéry and J. Harrowfield, *Inorg. Chem.*, 2015, **54**, 6296-6305.
30. W. Yang, T. G. Parker and Z. M. Sun, *Coord. Chem. Rev.*, 2015, **303**, 86-109.
31. Y. Yu, W. Zhan and T. E. Albrecht-Schmitt, *Inorg. Chem.*, 2007, **46**, 10214-10220.

32. *SAINT,* Bruker AXS Inc., Madison, Wisconsin, USA, 2007.
33. *APEX II,* Bruker AXS Inc., Madison, Wisconsin, 2008.
34. L. Krause, R. Herbst-Irmer, G. M. Sheldrick and D. Stalke, *J. Appl. Crystallogr.*, 2015, 3-10.
35. L. Palatinus and G. Chapuis, *J. Appl. Crystallogr.*, 2007, **40**, 786-790.
36. A. Altomare, G. Cascarano, C. Giacovazzo, A. Guagliardi, M. C. Burla, G. Polidori and M. Camalli, *J. Appl. Crystallogr.*, 1994, **27**, 435.
37. G. M. Sheldrick, *Acta Crystallogr. C Struct. Chem.*, 2015, **71**, 3-8.
38. L. J. Farrugia, *J. Appl. Crystallogr.*, 2012, **45**, 849-854.
39. A. L. Spek, *J. Appl. Crystallogr.*, 2003, **36**, 7-13.
40. C. F. Macrae, P. R. Edgington, P. McCabe, E. Pidcock, G. P. Shields, R. Taylor, M. Towler and J. van de Streek, *J. Appl. Crystallogr.*, 2006, **39**, 453-457.
41. *Crystal Maker*, Crystal Maker Software Limited, Bicester, England, 2009.
42. H. Putz and K. Brandenburg, *Match! - Phase Identification from Powder Diffraction*, **Crystal Impact: Bonn Germany, 2015.**
43. R. J. Batrice, J. A. Ridenour, R. L. Ayscue Iii, J. A. Bertke and K. E. Knope, *CrystEngComm*, 2017, **19**, 5300-5312.
44. C. Janiak, *J. Chem. Soc., Dalton Trans.*, 2000, 3885-3896.
45. K. P. Carter, S. J. A. Pope and C. L. Cahill, *CrystEngComm*, 2014, **16**, 1873.
46. J. A. Ridenour, K. P. Carter, R. J. Butcher and C. L. Cahill, *CrystEngComm*, 2017, **19**, 1172-1189.
47. J. A. Ridenour, K. P. Carter and C. L. Cahill, *CrystEngComm*, 2017, **19**, 1190-1203.
48. C. J. Kepert, L. Wei-Min, L. I. Semenova, B. W. Skelton and A. H. White, *Aust. J. Chem.*, 1994, **52**, 481-496.
49. K. P. Carter and C. L. Cahill, *Inorg. Chem. Front.*, 2015, **2**, 141-156.
50. K. P. Carter, M. Kalaj and C. L. Cahill, *Euro. J. Inorg. Chem.*, 2016, **2016**, 126-137.
51. S. G. Thangavelu, M. B. Andrews, S. J. A. Pope and C. L. Cahill, *Inorg. Chem.*, 2013, **52**, 2060-2069.
52. V. N. Serezhkin, M. S. Grigoriev, A. R. Abdulmyanov, A. M. Fedoseev, A. V. Savchenkov and L. B. Serezhkina, *Inorg. Chem.*, 2016, **55**, 7688-7693.
53. A. V. Savchenkov, A. V. Vologzhanina, L. B. Serezhkina, D. V. Pushkin and V. N. Serezhkin, *Polyhedron*, 2015, **91**, 68-72.
54. S. J. Jennifer and P. T. Muthiah, *Inorg. Chim. Acta*, 2014, **416**, 69-75.
55. V. V. Klepov, L. B. Serezhkina, A. V. Vologzhanina, D. V. Pushkin, O. A. Sergeeva, S. Y. Stefanovich and V. N. Serezhkin, *Inorg. Chem. Comm.*, 2014, **46**, 5-8.
56. P. Li, N. A. Vermeulen, X. Gong, C. D. Malliakas, J. F. Stoddart, J. T. Hupp and O. K. Farha, *Angew. Chem.*, 2016, **128**, 10514-10518.
57. J. Wang, Z. Wei, F. Guo, C. Li, P. Zhu and W. Zhu, *Dalton Trans.*, 2015, **44**, 13809-13813.
58. M. Kalaj, K. P. Carter, A. V. Savchenkov, M. M. Pyrch and C. L. Cahill, *Inorg. Chem.*, 2017, **56**, 9156-9168.
59. K. P. Carter, M. Kalaj, R. G. Surbella III, L. C. Ducati, J. Autschbach and C. L. Cahill, *Chem. Eur. J.*, 2017, **23**, 15355-15369.
60. M. L. Brown, J. S. Ovens and D. B. Leznoff, *Dalton Trans.*, 2017, **46**, 7169-7180.
61. A. de Bettencourt-Dias, P. S. Barber and S. Viswanathan, *Coord. Chem. Rev.*, 2014, **273–274**, 165-200.

62. H.-R. Mürner, E. Chassat, R. P. Thummel and J.-C. G. Bünzli, *J. Chem. Soc., Dalton Trans.*, 2000, 2809-2816.
63. C. Freund, W. Porzio, U. Giovanella, F. Vignali, M. Pasini, S. Destri, A. Mech, S. Di Pietro, L. Di Bari and P. Mineo, *Inorg. Chem.*, 2011, **50**, 5417-5429.
64. Y. G. Sun, B. Jiang, T. F. Cui, G. Xiong, P. F. Smet, F. Ding, E. J. Gao, T. Y. Lv, K. Van den Eeckhout, D. Poelman and F. Verpoort, *Dalton Trans.*, 2011, **40**, 11581-11590.
65. E. E. S. Teotonio, M. C. F. C. Felinto, H. F. Brito, O. L. Malta, A. C. Trindade, R. Najjar and W. Strek, *Inorg. Chim. Acta*, 2004, **357**, 451-460.
66. K. Binnemans, *Chem. Rev.*, 2009, **109**, 4283-4374.
67. P. M. Cantos, L. J. Jouffret, R. E. Wilson, P. C. Burns and C. L. Cahill, *Inorg. Chem.*, 2013, **52**, 9487-9495.
68. R. C. Severance, S. A. Vaughn, M. D. Smith and H.-C. zur Loye, *Solid State Sci.*, 2011, **13**, 1344-1353.
69. R. G. Denning, *J. Phys. Chem. A*, 2007, **111**, 4125-4143.
70. L. S. Natarajan, *Coord. Chem. Rev.*, 2012, **256**, 1583-1603.
71. A. de Bettencourt-Dias, *Dalton Trans*, 2007, 2229-2241.
72. J.-C. G. Bünzli and C. Piguet, *Chem. Soc. Rev.*, 2005, **34**, 1048-1077.
73. K. Binnemans, *Coord. Chem. Rev.*, 2015, **295**, 1-45.
74. R. G. Surbella III, M. B. Andrews and C. L. Cahill, *J. Solid State Chem.*, 2016, **236**, 257-271.
75. G. K. Liu and M. P. Jensen, *Chem. Phys.* , 2010, **499**, 178-181.
76. R. G. Surbella III, L. C. Ducati, J. Autschbach, N. P. Deifel and C. L. Cahill, *Inorg. Chem.*, 2018, **57**, 2455-2471.
77. K. Binnemans, *Chem. Rev.*, 2007, **107**, 2592-2614.
78. S. Tsushima, *Dalton Trans.*, 2011, **40**, 6732-6737.
79. Q. Liu, Q. Zhang, S. Yang, H. Zhu, Q. Liu and G. Tian, *Dalton Trans.*, 2017, **46**, 13180-13187.
80. G. Herzberg, *Infrared and Raman Spectra of Polyatomic Molecules*, D. Van Nostrand Company, Inc., New York, NY, 1946.
81. K. Nakamoto, *Infrared and Raman Spectra of Inorganic and Coordination Compounds Part A: Theory and Applications in Inorganic Chemistry*, John Wiley & sons, Inc., New York, NY, 5th, ed. edn., 1997.
82. S. P. McGlynn, J. K. Smith and W. C. Neely, *J. Chem. Phys.*, 1961, **35**, 105-116.
83. C. Nguyen-Trung, G. M. Begun and D. A. Palmer, *Inorg. Chem.*, 1992, **31**, 5280-5287.
84. L. H. Jones and R. A. Penneman, *J. Chem. Phys.*, 1953, **21**, 542-544.
85. F. Quiles, C. Nguyen-Trung, C. Carteret and B. Humbert, *Inorg. Chem.*, 2011, **50**, 2811-2823.
86. S. Fortier and T. W. Hayton, *Coord. Chem. Rev.*, 2010, **254**, 197-214.
87. M. Basile, D. K. Unruh, L. Streicher and T. Z. Forbes, *Cryst. Growth Des.*, 2017, **17**, 5330-5341.
88. L. M. Toth and G. M. Begun, *J. Chem. Phys.*, 1981, **85**, 547-549.
89. P. G. Allen, J. J. Bucher, D. L. Clark, N. M. Edelstein, S. A. Ekberg, J. W. Gohdes, E. A. Hudson, N. Kaltsoyannis, W. W. Lukens, M. P. Neu, P. D. Palmer, T. Reich, D. K. Shuh, C. D. Tait and B. D. Zwick, *Inorg. Chem.*, 1995, **34**, 4797-4807.

Concomitant and semi-selective uranyl and lanthanide luminescence observed within a series of f-f bimetallic molecular materials (UO_2^{2+} / Ln = Pr-Er).